Hindawi
Structural Control and Health Monitoring
Volume 2023, Article ID 4676060, 14 pages
https://doi.org/10.1155/2023/4676060

Research Article

Nonintrusive Sensor System Developed Using a Force-Sensing Resistor for Pipeline Integrity Monitoring

Jin-woo Park,[1] Byung Chang Jung,[1] Sang Hyuk Lee,[1] Young Cheol Huh,[1] and Yun-ho Shin[2]

[1]*Department of System Dynamics, Korea Institute of Machinery & Materials, Yuseong-gu, Daejeon 34103, Republic of Korea*
[2]*Department of Naval architecture & Ocean Engineering, Pusan National University, Geumjeong-gu, Busan 46241, Republic of Korea*

Correspondence should be addressed to Yun-ho Shin; shinyh77@pusan.ac.kr

Received 10 October 2022; Revised 30 December 2022; Accepted 11 January 2023; Published 7 February 2023

Academic Editor: Francesc Pozo

Pipelines are crucial for transporting liquid and gaseous resources at various industrial sites. As unexpected pipeline failures and improper spill responses often cause detrimental effects on the environment and public safety, real-time leakage monitoring and detection are important. This study proposes a nonintrusive sensor system to measure the pressure and integrity of a pipeline in real time by easily installing nonintrusive sensors on the exterior of the pipelines. Initially, a prototype of the nonintrusive pressure-monitoring sensor was designed and fabricated. This sensor correlated the changes in pressure inside a pipe with those in the contact force exerted between the pipe and the surrounding high-stiffness band; a force-sensing resistor was used to measure the contact force. Furthermore, parametric studies were performed on a six-inch pipe, which indicated that the developed sensor can accurately monitor the inner pressure of the pipe. We also developed a methodology to determine the optimal sensor placement in a pipeline network for detecting damages using the Euclidean distance method. This was combined with the methodology of determining the decision boundary for classifying the damage location using a support vector machine to rapidly detect the damage using a minimum number of sensors. Finally, a nonintrusive sensor system was installed on the fire main pipeline system, and the damage detection performance was experimentally validated. The developed nonintrusive sensor system can be easily installed on operating pipes to monitor the inner pressure of a pipe in real-time and accurately detect damages in a pipeline network.

1. Introduction

Pipelines, including peripherals such as pumps and valves, are instrumental in transporting liquid and gaseous resources at various industrial sites. Unexpected pipeline failures and improper spill responses often adversely affect the environment and public safety. Therefore, real-time leakage and rupture monitoring and detection are essential [1]. The methods for monitoring and analyzing pipeline integrity can be classified into two categories. The first method uses intrusive-type sensor systems that are based on the predesign and installation of a piping system; the second method uses nonintrusive sensor systems that can be easily applied to an existing pipeline system without modifying the target system [2].

Monitoring techniques for pipeline integrity using intrusive sensor systems include approaches based on mass/volume balance [3], pressure point analysis [4], and negative pressure wave analysis [5, 6]. Various physical measures, such as pressure, mass flow, and temperature of a piping system, have been introduced to realize these approaches. Although the integrity of piping systems can be accurately predicted by these approaches, their application involves certain challenges because the pressure or mass flow sensors should be pre-installed during the design and construction of the piping systems. Techniques using nonintrusive sensor

systems include external pressure monitoring, laser scanning, vision-based measurements, sound and vibration signal analysis [7–9], optical fiber measurements [4, 10, 11], and other related methods [12, 13]. Approaches based on vision, such as laser scanning and closed-circuit television, incur high initial installation expenses and exhibit restrictive environmental conditions based on the location of their installation on the pipeline systems. The system using sound and vibration signals is relatively convenient to install and can effectively identify damage and leakage of pipes; however, it is influenced by the surrounding noise. Therefore, it requires high-frequency sampling and high-specification data acquisition systems (DAQs). Conversely, optical fiber sensors can detect accurate leakage locations relatively well; nevertheless, a disadvantage is that all optical fibers require replacement when only a few of the fibers attached to the pipes are damaged. Although an approach using the fiber Bragg grating temperature-sensing method has been proposed to improve the cost and accuracy of optical fiber sensors, it cannot overcome the aforementioned limitations [14]. Recently, approaches using acoustic emissions and neural networks combined with artificial intelligence theory have been proposed. These methods require further investigations in terms of practical use and design generalization [15].

Among different pipeline systems applied in various industrial fields, naval ship pipeline systems, such as fire-extinguishing and cooling systems, are exposed to lethal damage conditions as they are subjected to projectile launches and collisions. The damage caused to fire-extinguishing and cooling systems can drastically reduce the mission capability. Therefore, to improve the sustainability of naval ships and crews, certain techniques must be employed for rapid damage detection and effective initial responses. In terms of detecting the damage caused to a mechanical system, several studies have performed conditional analysis and lifecycle prediction, including pipeline system leakage detection using machine learning and deep learning [16–18]. The support vector machine (SVM), a representative machine learning algorithm, was proposed in the early 1990s [19] and was applied to pattern classification and modeling fields, such as face recognition and failure analysis; the technique exhibited excellent performance [20, 21]. In subsequent studies, an appropriate property feature was selected to achieve the best performance of SVM, suitable for a specific environment and purpose based on the principal component analysis [22, 23].

This study proposes a novel system for pipeline integrity monitoring using a nonintrusive pressure-monitoring sensor with the advantages of a conventional nonintrusive method. The developed sensor detected the pressure inside a pipe using the contact force exerted between the pipe and the surrounding high-stiffness band. A force-sensing resistor (FSR) was used as the sensing material for measuring the contact force. Additionally, the optimal sensor placement in a pipeline network for detecting the damage was analyzed using the Euclidean distance method. Furthermore, we developed a methodology to determine the decision boundary for classifying the damage location using SVM and to rapidly detect the damage using a minimum number of sensors. Finally, the nonintrusive sensor system was installed on a land-based test facility, which simulated the rupture status of a pipeline system, namely, the fire main in a naval ship. The results indicated that the proposed system can perform excellently in practical applications.

The remainder of this paper is organized as follows: Section 2 describes the concept, specification, and prototype of the nonintrusive pressure-monitoring sensor. In Section 3, the methodology for designing the sensor placement in a pipeline network is presented, and the effectiveness of the developed nonintrusive sensor system is examined by applying it to the land-based test facility involving a fire main system. Finally, Section 4 summarizes the study findings.

2. Development of the Nonintrusive Pressure-Monitoring Sensor

2.1. Concept and Prototype. We designed and implemented a prototype of a nonintrusive pressure-monitoring sensor for a six-inch testbed pipe. Figure 1 depicts the nonintrusive pressure-monitoring sensor composed of a clamping band, force sensor, jig for locating the force sensor, and an operating circuit. The nonintrusive sensor was designed for a full-scale piping system considering the commercialization of the developed sensor system, and its details, including a clamping band, are summarized in Table 1. The considered target piping system is the one applied to frigates with the highest number of acquisitions among new class naval ships. The pipe diameter of the fire main used in this 3000-ton ship was 150 mm, and the thickness was 3 mm, so the sensor was designed and developed based on them. The clamping band comprised four links that were easily installed on the pipes; one of them had a groove for installing the force sensor and jig. The FSR was employed as a force sensor owing to its wide dynamic range, low cost ($10 per resistor), high energy efficiency because of a simple operating circuit, thinness, and flexibility in terms of installation on circular pipes. The sensing part of the FSR comprised a nonconductive polymer with conductive particles and two film-type electrodes (Figure 2). Typically, FSR relates force to resistance based on the quantum tunneling effect [2]. When a mechanical force is applied across the FSR, as indicated at the bottom of Figure 2, the tunneling paths (particle paths for electron transmission) are compressed. The compressed paths of conductive particles enable the flow of electrons between nonconductive polymers, thereby decreasing the resistance with an increase in the compression force [24]. FlexiForce A301 (Tekscan) was selected as the commercialized FSR for the prototype sensor owing to its excellent linearity, durability, precision, and pressure range in the testbed pipeline system [25]. Table 2 summarizes its specifications [25].

Figure 3 depicts the sensing part of the nonintrusive pressure-monitoring sensor, which comprises the FSR and the jig for locating the FSR. The jig included a rigid block and a button. The bottom of the rigid block was identical to the curvature of a pipe, and the top of the block was engraved similar to the external shape of FSR; this ensured that FSR was firmly attached during its installation on the pipe. The rigid

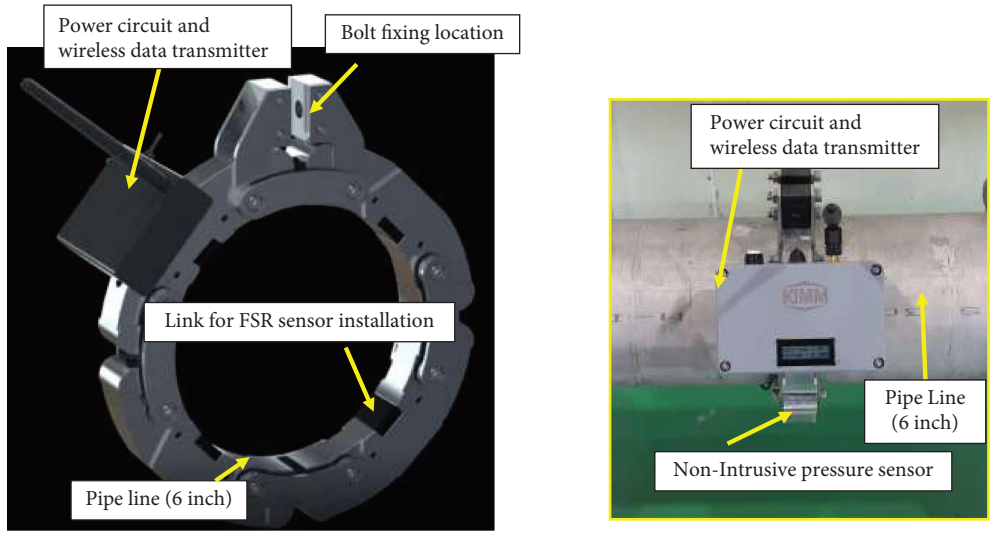

Figure 1: Design of the proposed nonintrusive pipeline pressure-monitoring sensor.

Table 1: Specifications of the pipe and band sensor.

	Parameter	Value
Pipe	Diameter	150 mm (6 in)
	Thickness	3 mm (SCH10)
	Material	SUS 304
	Usage pressure	Max. 10 bar
Clamping band	Diameter	166 mm
	Thickness	33 mm
	Material	AL6061

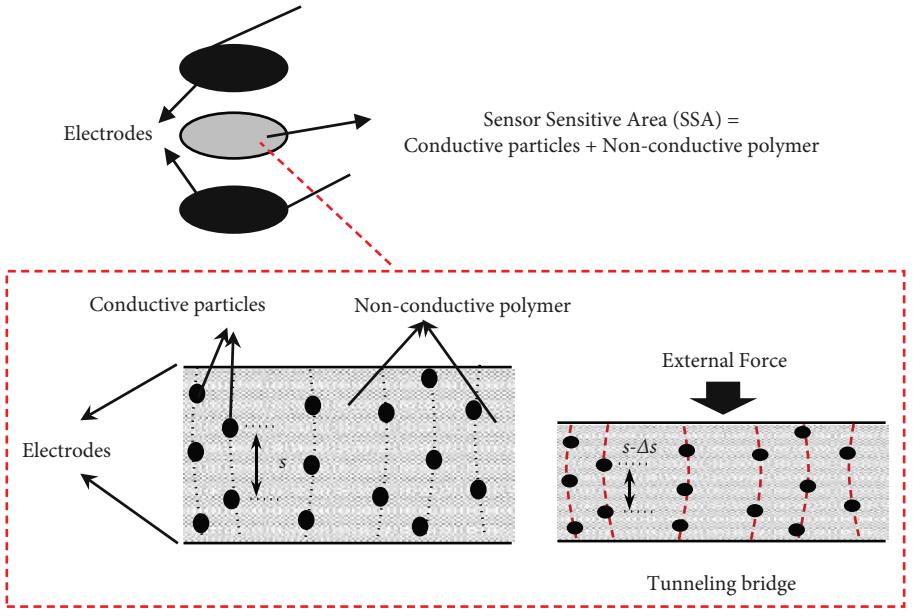

Figure 2: Operating principle of the force-sensing resistor (FSR).

button defined the optimal sensing area (A_{sensor}) of the FSR and generated a stable output by uniformly guiding the distributed normal force during its installation on the curved pipe. Figure 3 indicates that the optimal diameter of the rigid button was 7 mm, which was determined by a parametric study.

Figure 4 depicts the operating circuit designed to measure the output voltage by changing the resistance of the FSR. To improve the measurement accuracy and repeatability, the operating circuit was designed using three components, as indicated in the figure: (1) a voltage divider

Table 2: Specifications of FlexiForce A301.

Parameter	Value
Force range	4.445 N
Thickness	0.203 mm
Length	25.4 mm
Width	14 mm
Sensing area	9.53 mm diameter
Linearity (error)	<±3% of full scale
Repeatability	<±2%
Hysteresis	<4.5% of full scale
Drift	<5% per logarithmic time scale
Temperature sensitivity	0.36%/°C

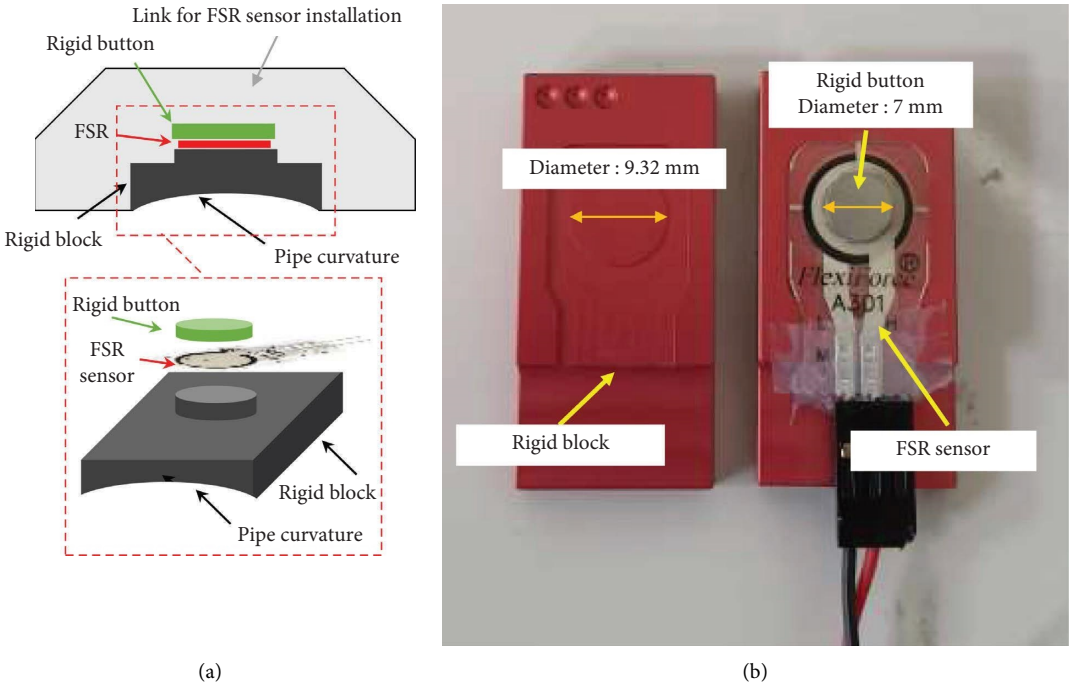

Figure 3: Sensing part of the nonintrusive pressure-monitoring sensor. (a) Concept of the sensing part with the force-sensing resistor (FSR) and jig for locating the FSR. (b) Photograph of the sensing part.

circuit (dotted box #1) with standard resistance (R_{ref}) and FSR resistance (R_{FSR}); (2) an operating amplifier (dotted box #2) to stabilize the output voltage in the voltage distribution circuit; and (3) a maximum output voltage of 5 V (dotted box #3). The transfer function of the operating circuit can be calculated using equation (1), as follows:

$$V_{out} = \left(1.107 \times \left(1 + \frac{R_{ref}}{R_{FSR}}\right) \times V_{ref}\right) - V_{ref}. \quad (1)$$

The standard resistance (R_{ref}) is a crucial parameter for determining the sensitivity of FSR. The sensitivity of the output voltage to the applied force changes according to the value of R_{ref} (Figure 5). Considering an initial clamping force of 300 N and the possible range of applied force as 0–200 N in the FSR measurement on a pipe, R_{ref} was set to 100 kΩ, the initial output voltage was 3.0 V, and the measurement voltage range was 3.0–5.0 V.

2.2. Performance Test. Figure 6 depicts the testbed that was built to experimentally verify whether the nonintrusive pressure-monitoring sensor can accurately predict the inner pressure of the pipe. An 80-cm-long pipe with a diameter of 6 inches was attached to the jig. The air pump was connected to increase the pressure in the pipe to 6 bar. The nonintrusive pressure-monitoring sensor was clamped onto the pipe and connected to a DAQ (QuantumX MX1615B, HBM). For comparison, an intrusive pressure sensor (WIKA S10, WIKA) was also installed to measure the actual pressure in the pipe. The sampling frequency of DAQ was set to 50 Hz.

The verification test was performed as follows: initially, the pressure in the pipe was set to 6 bar, which was reduced to 1 bar at intervals of 0.5 bar. Furthermore, the pressure was reduced from 1 to 0 bar at intervals of 0.1 bar. Figure 7 and Table 3 present the values of pressure in a pipe measured using intrusive and nonintrusive pressure sensors.

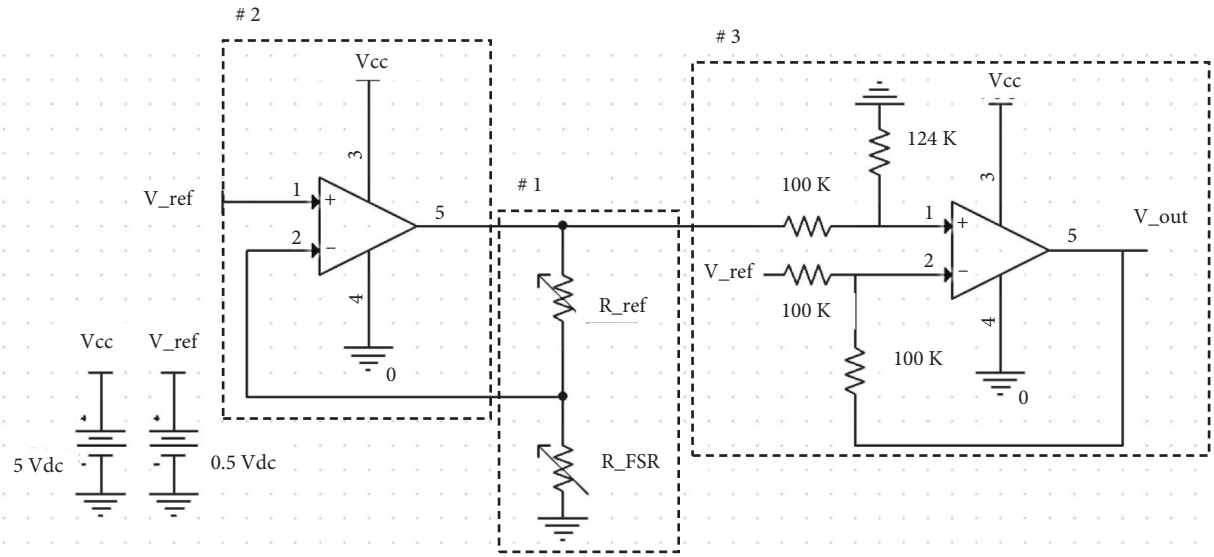

Figure 4: Operating circuit of the nonintrusive pressure-monitoring sensor.

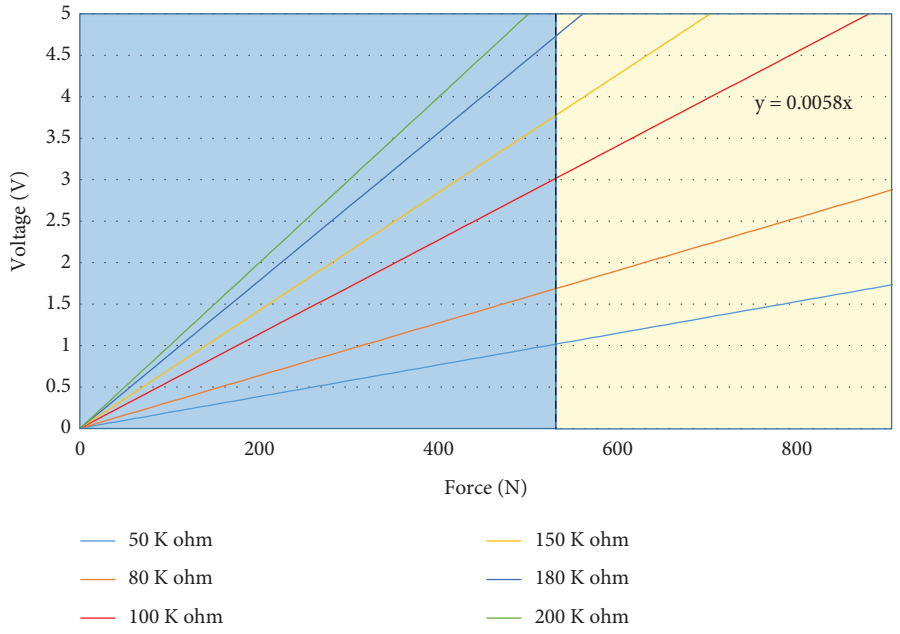

Figure 5: Sensitivity curves (output voltage to the applied force) based on the variation of the standard resistance (R_{ref}).

The results confirmed that both the developed sensor and the commercial sensor accurately predicted the pressure change in a pipe. The correlation coefficient between two sensors was very high at 0.994. Errors in predicting the pressure were less than 5.9% (0.154 bar) and 10.6% (0.038 bar) above and below 1 bar, respectively. As the reference pressure decreased, the percentage errors increased due to the digitizing noise.

3. Design Procedure of the Pipe Integrity Monitoring System

3.1. Sensor Placement Based on the Euclidean Distance Method. A design procedure was developed for sensor placement in a pipeline system to maximize the detectability of damages. The steps involved in the procedure can be summarized as follows:

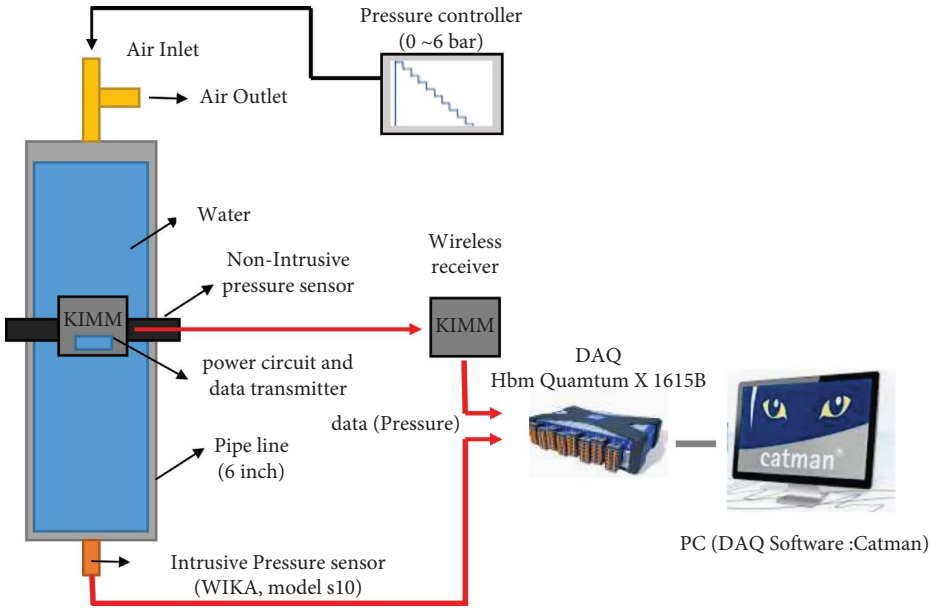

(a)

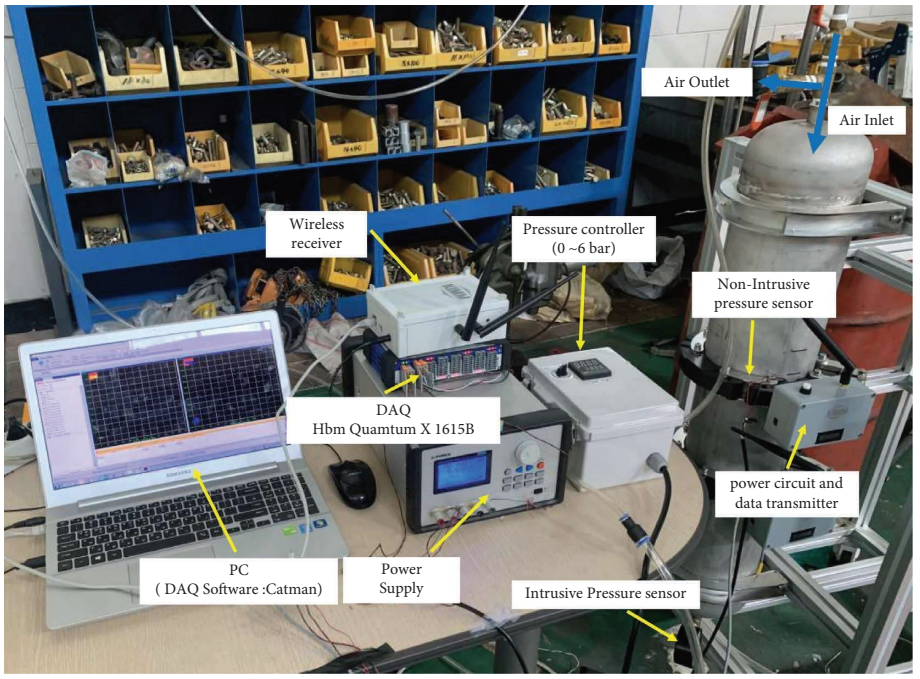

(b)

Figure 6: Experimental setup for testing the performance of the nonintrusive pipeline pressure-monitoring sensor. (a) Schematic of the experimental setup. (b) Photograph of the experimental setup.

(1) The damaged sections and the number of damaged sections (N_s) in the pipeline system were defined.

(2) Candidate sensor locations and the number of candidate locations (N_c) for sensor placement on the pipeline system were determined by considering the impediments of the pipeline system in terms of installation, such as flanges, valves, and supports.

(3) A flow analysis model was developed to predict the pressure at candidate sensor locations when the damage occurred in the pipeline system.

(4) The number of sensors (N_s) and the combination of candidate sensor locations to be installed on the pipeline system were defined. The number of combinations was calculated as $C(N_c, N_s) = N_c!/N_s!(N_c - N_s)!$.

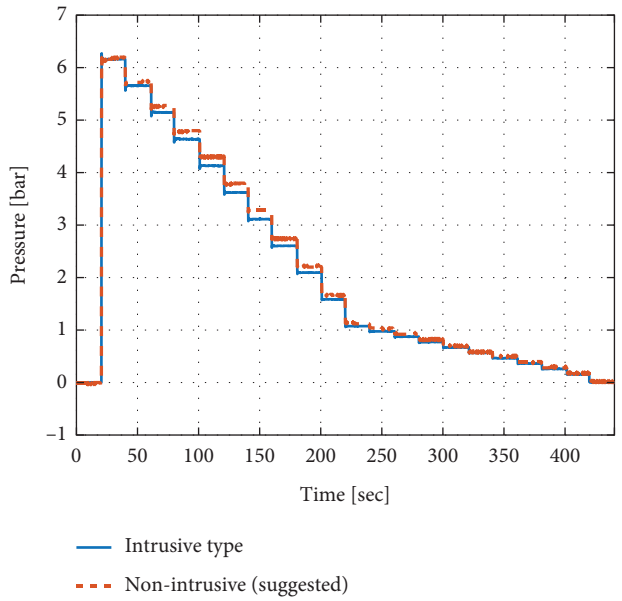

Figure 7: Comparison of the pressures measured by intrusive and nonintrusive sensors.

Table 3: Pressure measured using intrusive and nonintrusive sensors.

Intrusive sensor (bar)	Nonintrusive sensor (bar)	Gap	%
6.16	6.19	0.029	0.5
5.66	5.72	0.063	1.1
5.15	5.28	0.133	2.6
4.64	4.80	0.159	3.4
4.13	4.28	0.156	3.8
3.62	3.80	0.175	4.8
3.11	3.28	0.170	5.5
2.61	2.76	0.154	5.9
2.09	2.20	0.106	5.1
1.59	1.68	0.093	5.8
1.07	1.12	0.045	4.2
0.97	1.04	0.065	6.7
0.87	0.92	0.048	5.5
0.77	0.80	0.033	4.3
0.67	0.72	0.051	7.7
0.57	0.60	0.031	5.5
0.46	0.48	0.018	3.9
0.36	0.40	0.038	10.6
0.26	0.29	0.027	10.3
0.16	0.16	0.004	2.3
0.00	0.00	0.000	0.0

(5) The Euclidean distance (d) was calculated using the pressure values predicted by the combination of candidate sensor locations between the damages. For instance, the Euclidean distance between the pressure on damage 1 (p^1) and the pressure on damage 2 (p^2) can be calculated as follows:

$$d\left(p^1, p^2\right) = \sqrt{\left(p_1^1 - p_1^2\right)^2 + \left(p_2^1 - p_2^2\right)^2 + \cdots + \left(p_{N_s}^1 - p_{N_s}^2\right)^2}, \quad (2)$$

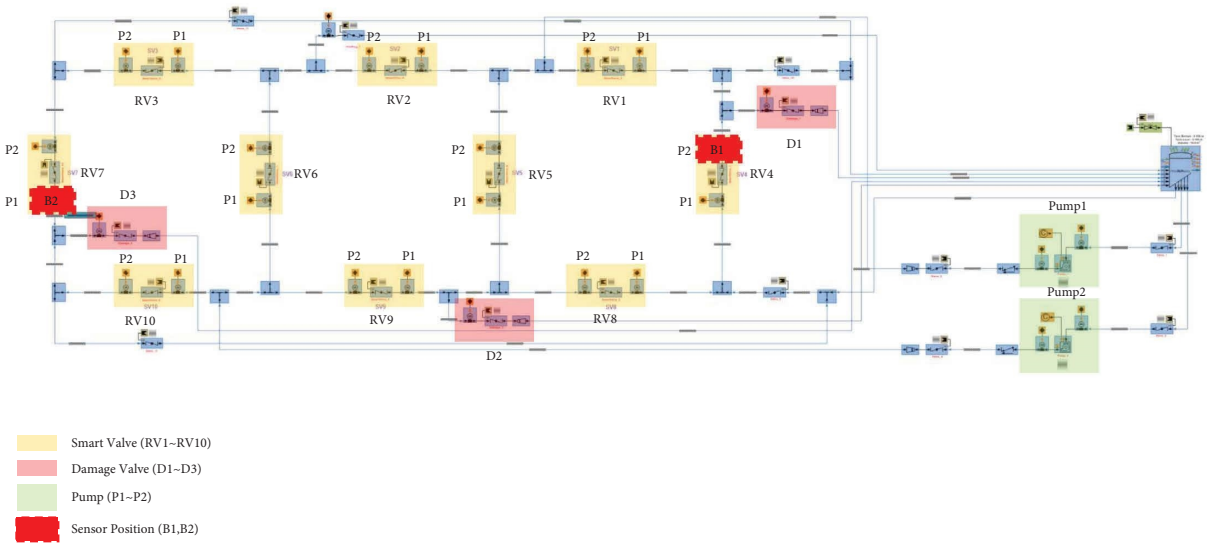

Figure 8: One-dimensional flow analysis model of the testbed pipeline system.

(6) Detectability was calculated by adding all Euclidean distances between damages. For example, for three damages, detectability can be obtained as $d(p^1, p^2) + d(p^1, p^3) + d(p^2, p^3)$.

(7) The optimal sensor placement was identified, which exhibited higher detectability among the different combinations of candidate sensor locations.

Figure 8 illustrates the flow analysis model of the testbed pipeline system obtained using the commercial software SimSmart. The yellow, red, and green boxes in the figure represent the valves, damaged sections, and pumps, respectively. The details of the testbed are explained in Section 3.3. Three damaged sections, namely, D1, D2, and D3, were defined in the testbed, implying that the number of damaged sections (N_s) was three. The testbed comprised 10 remote-controlled valves (RV1–RV10), and candidate sensor locations were defined as the right-hand side (P1) and left-hand side (P2) pipes of the valves. Therefore, the number of candidate locations (N_c) for sensor placement was 20. Table 4 summarizes the predicted pressure values at candidate sensor locations under the three damage conditions (D1, D2, and D3). As the number of sensors (N_s) was set to two, the number of combinations was 190. Based on the Euclidean distance, sensor combination, and damage, optimal sensor placements with the highest detectability were determined as P2 of SV4 and P1 of SV7, indicated as B1 and B2 in Figure 8, respectively.

3.2. Damage Detection Algorithm Based on SVM. Two nonintrusive sensors were manufactured and installed at locations B1 and B2, which were identified as optimal (Section 3.1). To determine whether two nonintrusive sensors can detect or classify the damage conditions in the testbed pipeline, 15 repetitive tests were performed at each damage condition, and the pressure data measured using nonintrusive sensors were obtained. Figure 9 depicts the pressure profiles of the two sensors under damage condition D1. The testbed pipeline was pressurized to 9 bar using two pumps under normal conditions. After the occurrence of damage (pipe rupture), the pressure measured at B1 and B2 decreased abruptly (Figure 9). The first maximum peak pressure after the damage was considered a training dataset to classify the damage conditions.

SVM is a representative machine learning algorithm that can be used for classifying nonlinear data using kernel calculations [26]. As shown in Figure 10, the SVM identified an optimized hyperplane ($f(x)$), which classified a maximum margin by learning the labeled data. The margin indicated the distance from the decision boundary to the nearest vector. The decision plane was computed by considering the number of samples (Figure 10). When learning data are available for linear separation, the separation hyperplane can be defined using equation (3); the hyperplanes are referred to as support vectors.

$$y_i(Wx_i + b) - 1 \geq 0. \tag{3}$$

Ideally, two hyperplanes are required to maximize the margin ($L(W)$) between two planes. This leads to an optimization problem for the objective function described in equation (4) under the constraints in equation (3) to obtain two classes of hyperplanes.

$$L(W) = \min\left(\frac{1}{2}\|W\|^2\right). \tag{4}$$

When a random input pattern is provided as the training data to the main axis, the discriminant functions can be defined as follows:

$$f(x) = \sum a_i y_i K(x_i, y_i) + b, \tag{5}$$

where α_i denotes the Lagrange multiplier and K indicates the kernel function.

Figures 11(a) and 11(b) depict the training dataset and test dataset for each damage condition, where the trained classifier is depicted in pink (damage 1), blue (damage 2), and red

Table 4: Values of pressure on candidate sensor locations predicted based on the flow analyses.

Damage	*V*1		*V*2		*V*3		*V*4		*V*5		*V*6		*V*7		*V*8		*V*9		*V*10	
	P1 (bar)	P2 (bar)	P1 (bar)	P2 (bar)	P1 (bar)	P2 (bar)	P1 (bar)	P2 (bar)	P1 (bar)	P2 (bar)	P1 (bar)	P2 (bar)	P1 (bar)	P2 (bar)	P1 (bar)	P2 (bar)	P1 (bar)	P2 (bar)	P1 (bar)	P2 (bar)
D1	0.125	0.236	0.242	0.255	0.257	0.260	0.102	0.153	0.234	0.239	0.258	0.262	0.261	0.263	0.228	0.178	0.262	0.236	0.265	0.268
D2	0.263	0.279	0.276	0.277	0.277	0.278	0.256	0.240	0.277	0.229	0.276	0.270	0.278	0.280	0.214	0.230	0.273	0.211	0.281	0.280
D3	0.287	0.290	0.282	0.255	0.244	0.187	0.285	0.282	0.279	0.283	0.250	0.255	0.159	0.102	0.276	0.280	0.259	0.274	0.151	0.254

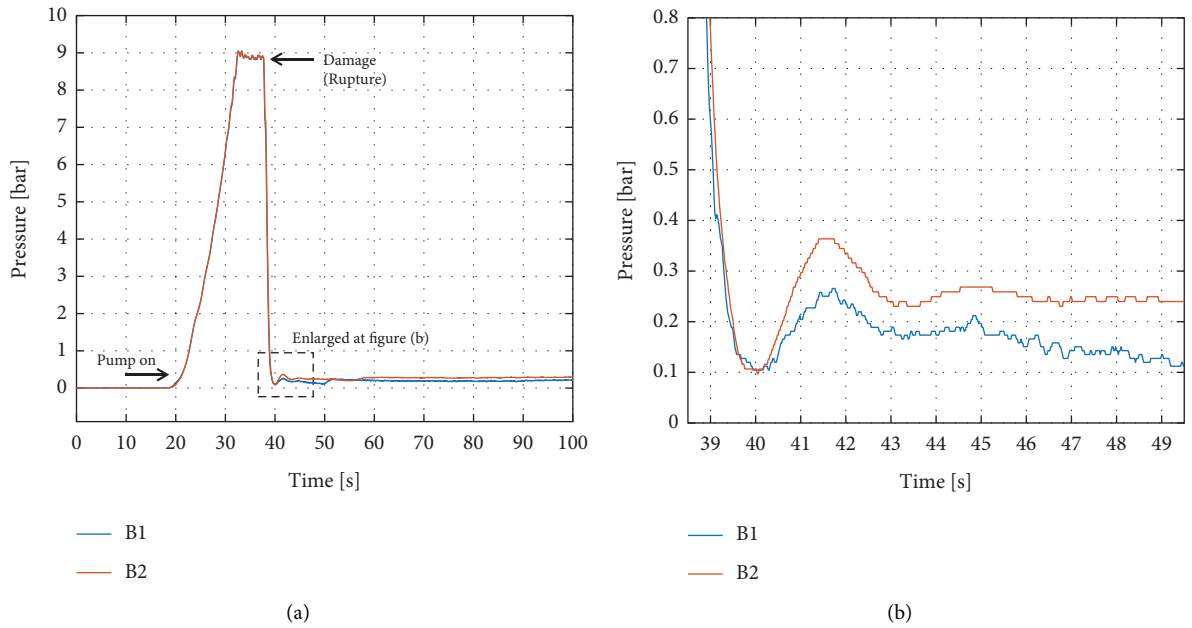

Figure 9: Pressure profiles before and after the pipe damage (D1): (a) 0~100 sec and (b) 38.5~49.5 sec.

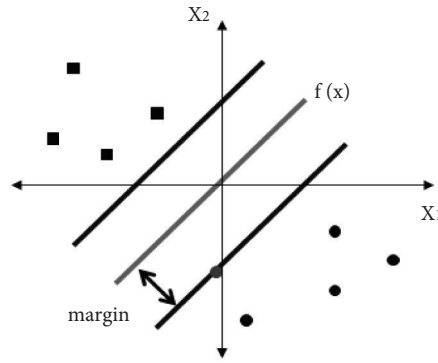

Figure 10: Basic concept of the support vector machine (SVM) method.

(damage 3) areas. Among the applicable kernel functions, such as linear, polynomial, and radial basis functions, a linear kernel was selected when designing the classifier using SVM as it was sufficient to identify the damage completely (100%) and simple to apply when realizing a commercial controller. In the case of the box constraint, the classifier was tuned to have an accuracy of 100% through trial and error because the classification of damage location is most important. The value was changed from 1 (default value) to 1000 after examination of the accuracy, and it was chosen as the value of 100, which shows the best performance.

3.3. Validations. The testbed was designed and constructed by referring to the fire main of an engine room and its adjacent compartments for a new 3000-ton class of naval ships from the Republic of Korea (ROK), and detailed specifications for the piping system are described in Table 5. Because the piping system of naval ships has a redundant design of pumps and piping equipment, a testbed that can realize pipeline damage (rupture) and consider redundancy was constructed in this research. Two centrifugal pumps to supply water for firefighting were connected to the right and left sides of the pipeline system. The damage (rupture) was simulated by opening the pressurized-air actuating valve installed at the predesigned location in the pipeline, as indicated in Figures 12(a) and 12(b). The water tank was designed with a volume of 22 m^3 to stably supply the excessive circulated flow induced by the rupture inside the pipeline.

Remote-controlled valves installed at the center of each pipeline segment were used to block the damaged pipeline section after detecting the damaged condition (D1, D2, or D3) using the proposed nonintrusive sensor system with the damage detection algorithm. Table 5 lists the specifications of the testbed.

The damage detection algorithm in the proposed nonintrusive sensor system with the hyperplane ($f(x)$) of the SVM was realized using a commercial controller

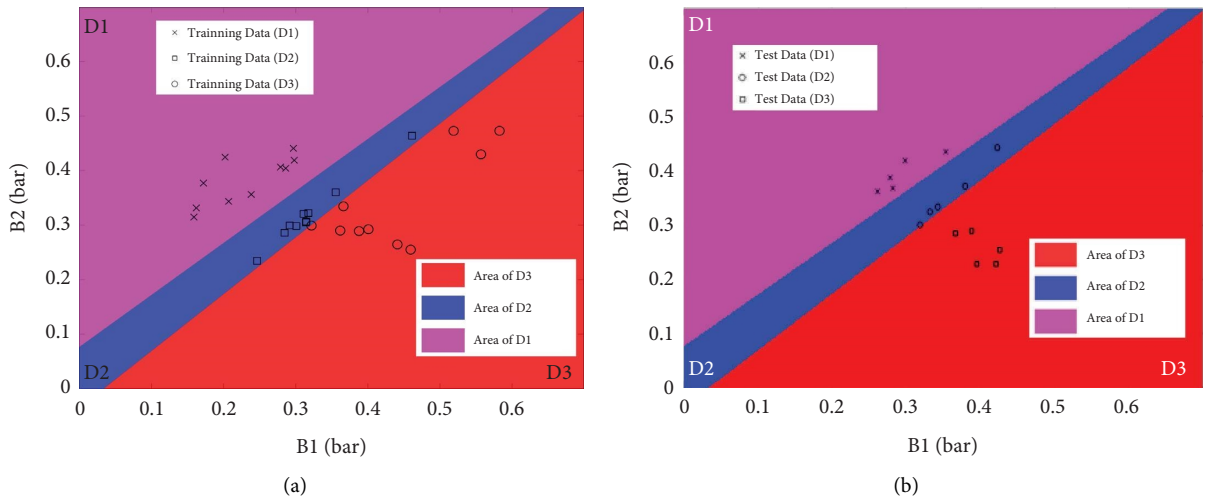

Figure 11: Decision boundary of the support vector machine. (a) Train dataset. (b) Test dataset.

Table 5: Specifications of the testbed pipeline system.

Item		Value	Remarks
Pipe system	Length (x)	12,000 mm	Overall dimension
	Width (Y)	8,000 mm	
	Height (Z)	2,500 mm	
	Pipe diameter	150 mm	Inner diameter
	Pipe thickness	3.4 mm	—
	Max. Pressure in pipe	9 bar	Operating pressure of firemain
Pump	Number	2 EA	—
	Type	Centrifugal horizontal multistage	—
	Maximum flow rate	114 m^3/h	—
Remote controlled butterfly valve		10 EA	Motor driven type
Damage valve for realizing pipeline rupture		3 EA	Air actuating type

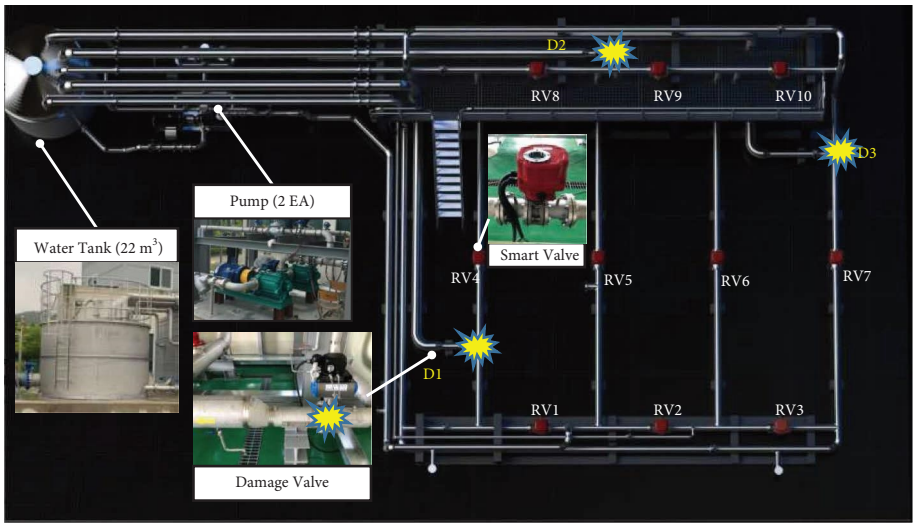

(a)

Figure 12: Continued.

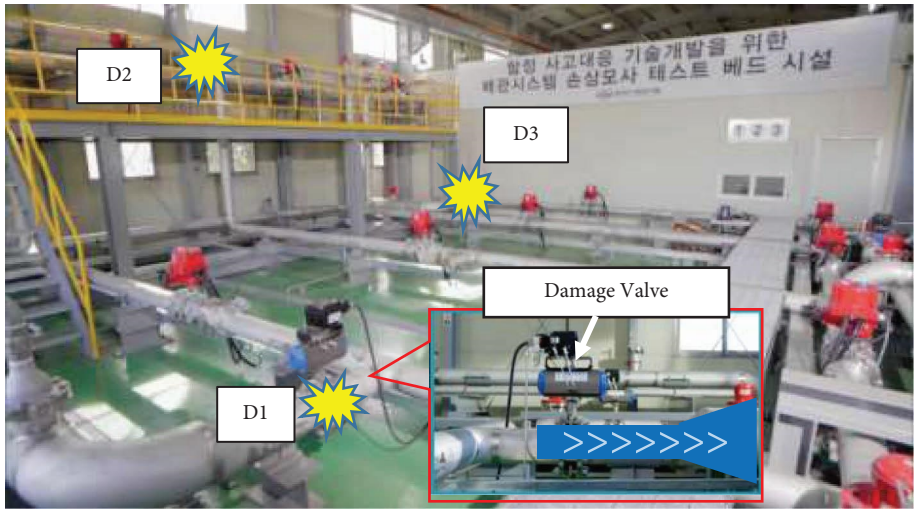

(b)

Figure 12: Configuration of the testbed pipeline system. (a) Top-view configuration. (b) Photograph.

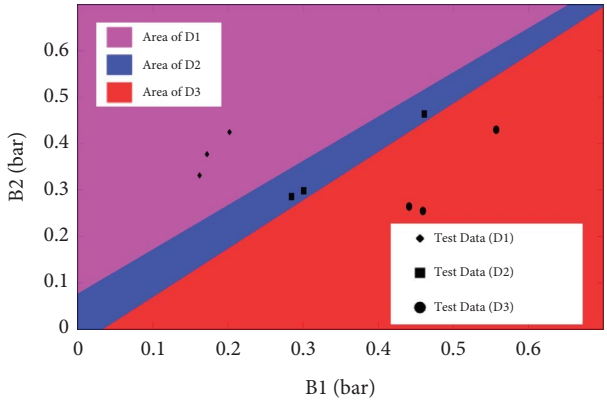

Figure 13: Performance test results of the nonintrusive sensor system.

(Arduino, board model: UNO R3), considering wireless communication. The performance of the proposed system was verified via three repetitive tests under three damage conditions. Nine tests were completed, and the results are plotted in Figure 13 along with the decision boundary of the proposed system. The experimental results indicated different patterns despite identical experimental conditions. This was because the flow fluctuated by approximately 10% under identical pump operating conditions within the controllable range of the test facility. The results verified that the proposed nonintrusive sensor system installed at the two locations in the piping system detected and classified all three types of damage situations and locations under feasible performance test conditions. Furthermore, the proposed design procedure for installing the nonintrusive sensor system was relatively convenient, without requiring any modification to the existing piping system. This methodology can be designed and applied to any piping system in an industry with a high risk of failure.

4. Conclusions

This study proposes a novel nonintrusive sensor system for monitoring pipeline pressure. We developed a methodology to determine the optimal location for the developed sensor in a pipeline network to detect the occurrence of leakages in the pipeline and perform the analysis in real time. A testbed was built for a nonintrusive sensor performance test, and a parametric study was performed to design the shape and operating circuit of the sensor for six-inch pipes. A wireless, nonintrusive pipeline pressure-monitoring sensor was fabricated based on the design parameters. The suggested sensor system installed on the pipe predicted pressure almost the same as the sensor installed inside the pipe, with a correlation coefficient of 0.994. Therefore, real-time monitoring of the pressure inside the pipe was feasible. The novel aspects of this study can be summarized as follows:

(i) Development of a nonintrusive pipeline pressure-monitoring sensor;

(ii) Methodology to determine the optimal sensor placement in a pipeline network for detecting damages using the Euclidean distance method;

(iii) Methodology to determine the decision boundary for classifying the damage location using SVM to rapidly detect damage; and

(iv) Performance evaluation of the nonintrusive pipeline pressure-monitoring sensor system using a real-scale land-based test facility for simulating the pipeline system of a conventional-class naval ship.

The proposed nonintrusive pipeline pressure-monitoring sensor system with the suggested design procedure showed excellent performance. In other words, the damage locations considered in this study were accurately classified, verifying that the proposed sensor can be applied to any piping system.

Data Availability

The data used to support this study are available from the corresponding author upon request.

Disclosure

Jin-woo Park and Byung Chang Jung contributed equally as co-first authors.

Conflicts of Interest

The authors declare that they have no conflicts of interest.

Authors' Contributions

Jin-woo Park was in charge of investigation, hardware, and software design, data curation, and writing the original draft. Byung Chang Jung handled methodology, algorithm development, and writing and editing the manuscript. Sang Hyuk Lee was in charge of validation and writing the manuscript; Young Cheol Huh handled data and study validation. Yun-ho Shin was in charge of conceptualization, supervision, organization, and writing and editing the manuscript.

Acknowledgments

This research was supported by the Basic Project of Korea Institute of Machinery and Materials (grant no. NK238B) and the Energy Demand Management Core Technology Development Project through the Korea Institute of Energy Technology Evaluation and Planning (KETEP) funded by the Ministry of Trade, Industry and Energy (grant no. 20212020900090). This research was also supported by the National Research Foundation of Korea (grant no. NRF-2022M1A2A2079987).

References

[1] Korea Ministry of Environment, *Statistics of Waterworks*, Korea Ministry of Environment, Sejong, South Korea, 2019.

[2] M. A. Adegboye, W. K. Fung, and A. Karnik, "Recent advances in pipeline monitoring and oil leakage detection technologies: principles and approaches," *Sensors*, vol. 19, no. 11, p. 2548, 2019.

[3] P. Ostapkowicz, "Leak detection in liquid transmission pipelines using simplified pressure analysis techniques employing a minimum of standard and non-standard measuring devices," *Engineering Structures*, vol. 113, pp. 194–205, 2016.

[4] L. Wang, S. C. Narasimman, S. Reddy Ravula, and A. Ukil, "Water ingress detection in low-pressure gas pipelines using distributed temperature sensing system," *IEEE Sensors Journal*, vol. 17, no. 10, pp. 3165–3173, 2017.

[5] Y. Sang, J. Zhang, X. Lu, and Y. Fan, "Signal processing based on wavelet transform in pipeline leakage detection and location," in *Proceedings of the 16th International Conference on Intelligent Systems Design and Applications*, vol. 2, pp. 734–739, IEEE, Jian, China, October 2006.

[6] Z. Yu, L. Jian, Z. Zhoumo, and S. Jin, "A combined kalman filter-discrete wavelet transform method for leakage detection of crude oil pipelines," in *Proceedings of the 9th International Conference on Electronic Measurement & Instruments*, pp. 1086–1090, IEEE, Beijing, China, August 2009.

[7] A. Martini, M. Troncossi, and A. Rivola, "Leak detection in water-filledsmall-diameter polyethylene pipes by means of acoustic emission measurements," *Applied Sciences*, vol. 7, no. 1, p. 2, 2016.

[8] S. Li, Y. Wen, P. Li, J. Yang, and L. Yang, "Leak detection and location for gas pipelines using acoustic emission sensors," in *Proceedings of the 2012 IEEE International Ultrasonics Symposium*, pp. 957–960, IEEE, Dresden, Germany, October 2012.

[9] P. Recommended, "DNVL-RP-F302," 2016, https://rules.dnvgl.com/docs/pdf/DNVGL/RP/2016-04/DNVGL-RP-F302.pdf.

[10] F. Tanimola and D. Hill, "Distributed fibre optic sensors for pipeline protection," *Journal of Natural Gas Science and Engineering*, vol. 1, no. 4-5, pp. 134–143, 2009.

[11] A. A. Khan, V. Vrabie, J. I. Mars, A. Girard, and G. D'Urso, "A source separation technique for processing of thermometric data from fiber-optic dts measurements for water leakage identification in dikes," *IEEE Sensors Journal*, vol. 8, no. 7, pp. 1118–1129, 2008.

[12] G. Park, H. H. Cudney, and D. J. Inman, "Feasibility of using impedance-based damage assessment for pipeline structures," *Earthquake Engineering & Structural Dynamics*, vol. 30, no. 10, pp. 1463–1474, 2001.

[13] C. Zuo, X. Feng, Y. Zhang, L. Lu, and J. Zhou, "Crack detection in pipelines using multiple electromechanical impedance sensors," *Smart Materials and Structures*, vol. 26, no. 10, Article ID 104004, 2017.

[14] C. Gong, S. Li, and Y. Song, "Experimental validation of gas leak detection in screwthread connections of galvanized pipe based on acousticemission and neural network," *Structural Control and Health Monitoring*, vol. 27, no. 1, pp. 1–12, 2019.

[15] M. Sun, B. Shi, D. Zhang, C. Feng, J. Wu, and G. Wei, "Pipeline leakage monitoring experiments based on evaporation-enhanced fbg temperature sensing technology," *Structural Control and Health Monitoring*, vol. 28, no. 3, p. 1~18, 2021.

[16] A. Mohamed, M. S. Hamdi, and S. Tahar, "A hybrid intelligent approach for metal-loss defect depth prediction in oil and gas pipelines," *Intelligent Systems and Applications*, pp. 1–18, Springer, Cham, Switzerland, 2016.

[17] Y. Ying, J. H. Garrett, J. Harley, I. J. Oppenheim, J. Shi, and L. Soibelman, "Damage detection in pipes under changing environmental conditions using embedded piezoelectric transducers and pattern recognition techniques," *Journal of Pipeline Systems Engineering and Practice*, vol. 4, no. 1, pp. 17–23, 2013.

[18] L. H. Lee, R. Rajkumar, L. H. Lo, C. H. Wan, and D. Isa, "Oil and gas pipeline failure prediction system using long range ultrasonic transducers and euclidean-support vector machines classification approach," *Expert Systems with Applications*, vol. 40, no. 6, pp. 1925–1934, 2013.

[19] C. Cortes and V. Vapnik, "Support-vector networks," *Machine Learning*, vol. 20, no. 3, pp. 273–297, 1995.

[20] T. B. Trafalis and H. Ince, "Support vector machine for regression and applications to financial forecasting," in *Proceedings of the IEEE-INNS-ENNS International Joint Conference on Neural Networks. IJCNN 2000. Neural Computing: New Challenges and Perspectives for the New Millennium*, pp. 348–353, Como, Italy, July 2000.

[21] W. S. Noble, "Support vector machine applications in computational biology," *Kernel methods in computational biology*, vol. 71, p. 92, 2004.

[22] E. W. T. Ngai, Y. Hu, Y. H. Wong, Y. Chen, and X. Sun, "The application of data mining techniques in financial fraud detection: a classification framework and an academic review of literature," *Decision Support Systems*, vol. 50, no. 3, pp. 559–569, 2011.

[23] J. D. Kelleher, B. Mac Namee, and A. D Arcy, "Fundamentals of machine learning for predictive data analytics: algorithms," *Worked Examples, and Case Studies*, MIT Press, Cambridge, UK, 2015.

[24] L. Paredes-Madrid, C. A. Palacio, A. Matute, and C. A. Parra Vargas, "Underlying physics of conductive polymer composites and force sensing resistors (FSRs) under static loading conditions," *Sensors*, vol. 17, no. 9, p. 2108, 2017.

[25] Tekscan, "Tekscan inc. Flexiforce, standard force & load sensors model A301," 2021, https://www.tekscan.com/products-solutions/force-sensors/a301.pdf.

[26] H. Shukla and K. Piratla, "Leakage detection in water pipelines using supervised classification of acceleration signals," *Automation in Construction*, vol. 117, Article ID 103256, 2020.